10^{th} International Conference on Fracture Mechanics of Concrete and Concrete Structures
FraMCoS-X
G. Pijaudier-Cabot, P. Grassl and C. La Borderie (Eds)
https://doi.org/10.21012/FC10.232780

MULTIPHYSICS LATTICE DISCRETE PARTICLE MODEL FOR THE SIMULATION OF CONCRETE THERMAL SPALLING

LEI SHEN*, WEIXIN LI†, XINWEI ZHOU‡, JUN FENG°, GIOVANNI DI LUZIO•, QINGWEN REN◇, AND GIANLUCA CUSATIS⋆

*Hohai University, Nanjing, Jiangsu China
e-mail: shenlei-hhu@foxmail.com

†Northwestern University, Evanston, IL USA
e-mail: lwx3000@gmail.com

‡ES3, San Diago, CA USA
e-mail: xinwei.zhou@es3inc.com

°Nanjing University of Science and Technology, Nanjing, Jiangsu China
e-mail: fengjun2016@hotmail.com

•Politecnico di Milano, Milan, Italy
e-mail: giovanni.diluzio@polimi.it

◇Hohai University, Nanjing, Jiangsu China
e-mail: renqw@hhu.edu.cn

⋆Northwestern University, Evanston, IL USA
e-mail: g-cusatis@northwestern.edu

Key words: concrete thermal spalling, high temperature, discrete, lattice discrete particle model, hygro-thermal coupling

Abstract. Explosive thermal spalling behavior during fire exposure is one of the major issues in the design of modern reinforced concrete structures. However, spalling mechanisms and their interaction still remain in dispute in the scientific community. In order to shed some light on this phenomenon, a discrete hygro-thermal model of concrete at high temperature called DTemPor3 is proposed and a full coupling scheme between DTemPor3 and the Lattice Discrete Particle Model (LDPM) is adopted. The proposed multi-physical coupled model features the effect of pore pressure and temperature on the mechanical response as well as the impact of cracking on moisture mass transport and heat transfer. This proposed model can reproduce the explosive spalling phenomenon and only when the effect of thermal stresses is taken in account along with the effect of pore pressure on crack initiation, as demonstrated by the numerical simulations.

1 INTRODUCTION

Concrete tends to be very sensitive to explosive spallling when it is exposed to fire and its sensitivity to this phenomenon must be considered and controlled in the design and construction of reinforced concrete structures, especially for the design of tunnels. As a result, thermal spalling of concrete has been a hot topic for the scientific community over the last

30 years. However, the main driving mechanisms are not completely clear due to the complex interaction of heat transfer, moisture mass transport, as well as mechanical and chemical behavior of concrete at high temperature. On the one hand, the pressure builds up in the concrete pores as a consequence of the physically and chemically bound water in the cement that vaporizes at high temperature, and it leads to tensile stresses in the heated concrete [1]. On the other hand, the restrained thermal dilation generate a biaxial state of stress with compressive stresses parallel to the heated surface and tensile stresses perpendicular to the heated surface [2]. Internal stresses build up as a result of the combined effect of pore pressure increase, thermal stresses derived from temperature gradients, mismatch between the deformation of different constituents, and the shrinkage associated with water release [3,4]. When the internal stresses exceed the maximum tensile strength, cracks and/or spalling occur.

Although some reasonable discussions on the various mechanisms were given in previous studies [5–7], there were no evident results persuading other researchers because the dynamic explosive fragmentation due to the spalling phenomena was not simulated correctly by the traditional continuous finite element approaches. Therefore, this study responds to an actual need for a reliable computational tool capable of simulating the dynamic explosive fragmentation during spalling.

In this study, a discrete temperature and pore vapor pressure model in 3D (called DTemPor3) is formulated and implemented within the framework of the Lattice Discrete Particle Model [9]. The spalling phenomena observed in the experiments [12] are reproduced and the main driving mechanisms are discovered.

2 The Computational Framework

2.1 The Lattice Discrete Particle Model at high temperature

The Lattice Discrete Particle Model (LDPM), originally formulated by Cusatis et al. [9], is able to accurately capture the failure behavior of concrete at room temperature as demonstrated in many previous studies. This study proposes an improvement of LDPM in order to allow the simulation of concrete behavior at high temperature.

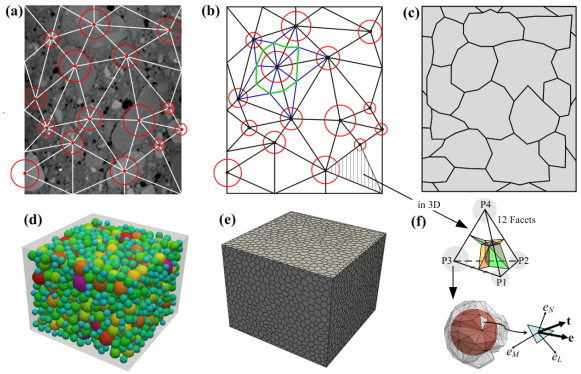

Figure 1: LDPM geometry. (a) Concrete mesostructure in 2D; (b) Delaunay triangulation in 2D; (c) LDPM cells in 2D; (d) LDPM particles in 3D; (e) LDPM cells in 3D; (f) LDPM facets.

LDPM simulates the concrete mesostructure by taking into account the interaction of coarse aggregate pieces. Coarse aggregate pieces with different size are randomly placed inside the concrete volume following the Fuller sieve curve. A typical aggregate distribution is shown in Fig. 1(a) in 2D and (d) in 3D. The Delaunay tetrahedralization is used to connect the centers (termed "nodes") of the spherical particles to produce tetrahedra. The edges of the tetrahedra form the lattice system that describes the interaction between adjacent particles as shown in Fig. 1(b) in 2D. A domain tessellation is performed to define a set of 12 potential failure locations (termed "facets") in each tetrahedron (see in Fig. 1(f)). The tessellation procedure is described in detail in Cusatis et al. [9]. By connecting the facets surrounding each aggregate center, a system of polyhedral cells is obtained as illustrated in Fig. 1(c) in 2D and (e) in 3D.

The facet strains between two adjacent Tet-nodes are defined as $\mathbf{e} = [e_N\ e_M\ e_L]^{\mathrm{T}}$, where $e_N = \mathbf{n}^{\mathrm{T}}[\![\mathbf{u}]\!]/l$ is the normal strain component, $e_M = \mathbf{m}^{\mathrm{T}}[\![\mathbf{u}]\!]/l$ and $e_L = \mathbf{l}^{\mathrm{T}}[\![\mathbf{u}]\!]/l$ are the tangential strain components, $[\![\mathbf{u}]\!]$ is the displacement jump at the centroid of the facet, l is the

tetrahedron edge associated with the facet and **n**, **m**, and **l** are unit vectors normal and tangential to each facet. By assuming additivity of strains, one can write:

$$\dot{\mathbf{e}} = \dot{\mathbf{e}}^s + \alpha_T \dot{T}\mathbf{n} \tag{1}$$

in which $\mathbf{e}^s$ represents stress-related strains and the term $\alpha_T \dot{T}$ represents the thermal expansion is the main impose normal strain, $\dot{T}$ is the temperature rate and $\alpha_T(T)$ is the thermal expansion coefficient which is an overall result of the cement shrinkage and aggregate dilatation occurring at high temperature [2].

The LDPM elastic behavior is described by assuming that the normal and shear tractions acting on the solid skeleton proportional to the corresponding strains. One can write $\mathbf{t}^s = [t^s_N\ t^s_M\ t^s_L]^{\mathrm{T}}$, where $t^s_N = E_N e^s_N$ is the normal component, $t^s_M = E_T e^s_M$ and $t^s_L = E_T e^s_L$ are the shear components; $E_N = E_0$, $E_T = \alpha E_0$, E_0 is the effective normal elastic modulus estimated by Young's modulus and Poisson's ratio. $\alpha = 0.25$ is the shear-normal coupling parameter. The detail constitutive relations describing the inelastic behavior are formulated in Cusatis et al. [9].

The mesoscopic crack opening vector associated with each facet can be calculated as $\boldsymbol{\delta} = \delta_N\mathbf{n}+\delta_L\mathbf{l}+\delta_M\mathbf{m}$, where $\delta_N = l\,(e^s_N - t^s_N/E_N)$, $\delta_L = l\,(e^s_L - t^s_L/E_L)$, $\delta_M = l\,(e^s_M - t^s_M/E_M)$. δ_N is its normal component, and δ_M and δ_L are two shear components related to the sliding of crack surfaces.

Thermal degradation in LDPM is introduced through the following function:

$$f_d = 1 - \frac{\exp(n_d)\Theta}{1 - \Theta(1 - \exp(n_d))} \tag{2}$$

where n_d is the parameter controlling the shape of the thermal degradation evolution and Θ is a temperature level variable, $\Theta = (\langle T - T_s\rangle)/(T_m - T_s)$, T_s is the temperature at which concrete starts to degrade and T_m is the temperature at which concrete starts to melt. LDPM material parameters, σ_t, σ_s, E_0, σ_{c0} and σ_{N0} are assumed to decay proportional to f_d in Tab. 1. The thermal degradation formulations are calibrated by unconfined uniaxial compression tests, triaxial compression tests, and tensile strength tests available in the literature. The tensile characteristic length (l_t) and all the other is assumed to remain constant.

Table 1: Thermal degradation of LDPM parameters

Parameters		T_s	T_m	n_d
Unit		[°C]	[°C]	[–]
σ_t	Tension strength	274	1000	0.4
σ_s	Compression strength	274	1000	0.4
E_0	Effective normal elastic modulus	20	1000	0.7
σ_{c0}	Compression yielding strength	340	1000	0.2
σ_{N0}	Transitional strength	340	1000	0.2

At high temperature, concrete internal stress is not only caused by the deformation but also by water or vapor pressure in the pores. Hence the total stress vector on each facet can be computed as:

$$\mathbf{t} = \mathbf{t}^s - bp\mathbf{n} \tag{3}$$

where, p is pore pressure and b is the Biot coefficient [13, 14] which is assumed to be equal to 1 unless otherwise mentioned in the current formulation [5]. Finally, equilibrium equations are obtained through the force and moment equilibrium of each cell surrounded by a group of facets. ge

2.2 The Hygro-Thermal model

Considering the discrete character, the hygro-thermal equations are formulated with reference to a 3D network of 1D elements anchored to the LDPM geometry [14]. Let's consider two Tet-points inside two adjacent LDPM tetrahedra labeled as node "T_1" and "T_2" in the 2D representation of Fig. 2 (a). The segment connecting T_1 and T_2 is called "Flow Lattice Element" (FLE_{12}). Each FLE has an associated volume, and the average of pore pressure

and temperature on "T_1" and "T_2" represent the mass thermodynamic state in the FLE_{12} domain volume. Accordingly, for each FLE, the mass and heat balance equations can be written as:

$$\frac{d}{dt}\left(V_{wi}w_w + V_{ci}w_c\right) = A_w\left(D_1\frac{p_2-p_1}{l_{12}} + D_2\frac{T_2-T_1}{l_{12}}\right) \quad (4)$$

$$\frac{d}{dt}\left(V_{wi}U_w + V_{ci}U_c\right) = A_w\left(D_3\frac{p_2-p_1}{l_{12}} + D_4\frac{T_2-T_1}{l_{12}}\right) \quad (5)$$

where, t is time; $p_i(t)$ and $T_i(t)$ are pore pressure and temperature at T_i, $(i = 1, 2)$; $V_w = \sum_1^2 V_{wi}$ is the FLE_{12} domain volume; $l_{12} = \sum_1^2 l_i$ is the FLE_{12} length and the superscript $i = 1, 2$ identify variables relevant to the Side T_1 and the Side T_2, respectively. In Fig. 2 (b), $\mathbf{a}$ is the unit vector orthogonal to the tetrahedron face $P_1P_2P_3$, and $\mathbf{e}$ is the direction of FLE_{12} from T_2 to T_1. The projection of the area $P_1P_2P_3$ ($A_\triangle$) in the $\mathbf{e}$ direction is defined as $A_w = -A_\triangle \mathbf{a}^{\mathrm{T}}\mathbf{e}$. One can write $V_w = l_{12}A_w/3$ and the domain volume increase is assumed to come from the initiation and propagation of cracks on the corresponding facets ($V_c = \sum_{i=1}^2\sum_{j=1}^3(\delta_{NPj}^i A_{FPj}^i)$) and the elastic volume increase of V_{wi} is neglected. δ_{NPj}^i denotes the normal crack opening of a facet connecting with T_i and A_{FPj}^i is the corresponding facet area.

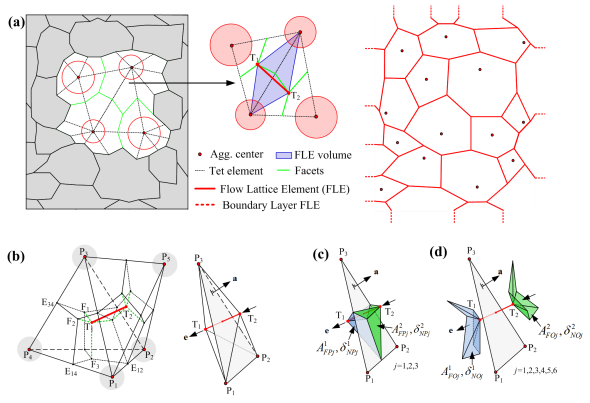

Figure 2: Flow Lattice Element (FLE) system geometry. (a) FLE generation in 2D. (b) FLE in 3D. (c) LDPM facets related to mass transport. (d) LDPM facets related to heat transfer.

$w_w(p, T)$ denotes the water mass per unit volume of uncracked material which can be divided into evaporable water (w_e), and water released by dehydration (w_d) at high temperature. The $w_e(T, p)$ is controlled by the desorption isotherms equilibrium curves presented by Bažant et al. [2]. The evaporable water content in concrete at high temperature can be expressed as a function of relative humidity ($h = p/p_{sat}(T)$). If $h \leqslant 0.96$, $w_e = c(hw_0/c)^{1/m_{iso}}$. If $h \geq 1.04$, $w_e = w_f[1 + 0.12(h - 1.04)]$. Otherwise, when $0.96 < h < 1.04$, $w_e = w_e^{1.04} - (w_e^{1.04} - w_e^{0.96})(1.04-h)/0.08$. In above, c is the cement content per unit volume of concrete, w_0 is the water content in unit volume of saturated concrete at 25 °C, $w_f = w_0 + w_d$ denotes water content in unit volume of saturated concrete at any temperature, m_{iso} is a temperature dependent coefficient defined as $m_{iso} = 1.04 - (T_C + 10)^2/[(T_C + 10)^2 + 22.3 \times 35^2]$. The pore pressure at saturation, p_{sat}, could be found in [7].

$w_d(T)$ gradually releases in the pores for temperatures ranging from 105 °C to 1000 °C. The empirical equation proposed by Gawin et al. [7] is used as evolution law for this process. If $T \leqslant 105°\mathrm{C}$, $w_d = 0$. Otherwise, when $T > 105°\mathrm{C}$, $w_d = 0.32\alpha_c^\infty c f_{wd}(T_{max}(t))$, in which, $\alpha_c^\infty = 1.032w_{mix}/c/(0.194 + w_{mix}/c)$ is the asymptotic hydration degree [15]; w_{mix} is the initial water in the concrete mix; T_{max} is the highest temperature reached by concrete during heating; $f_{wd}(T)$ is a dimensionless function of temperature which could be found in [7].

$U_w(p, T)$ denote the heat content per unit volume of uncracked material. It can be expressed as the algebraic sum of the heat density in the uncracked material and the heat consumption due to the dehydration. One can write as $U_w = U_s - U_d$, where $U_s = \rho_s C_s T$ is the heat density in uncracked material with the solid skeleton density $\rho_s = 2400\ \mathrm{kg/m^3}$, and the heat capacity $C_s = 900 + 80\,(T_C/120) - 4\,(T_C/120)^2$ [5]. The dehydration heat consumption is defined as $U_d = C_d w_d$, in which $C_d = 2400\ \mathrm{J/kg}$ is the heat consumption of dehydration per kilogram of concrete [2].

D_1 is the hydraulic conductivity (permeability) in Fick's Law and $D_2 = 0$ is the coefficient for Soret mass flux which is usu-

ally neglected due to its small contribution. Hence the effective permeability can be given as $D_1 = D_w + D_c$, in which D_w is the permeability of the uncracked material, $D_w = f_1(h)\, 10^{C_T(T-T_0)} D_w^0$, and D_c is the permeability due to the water flow in the cracks, formulated by postulating a Poiseuille flow, $D_c^i = \rho_c/(12\mu_c A_w) \sum_{i=1}^{3} l_{NPj} (\delta_{NPj}^i)^3$, where $f_1(h)$ is a function of relative humidity [2]; C_T is the a factor that accounts for the increase of permeability in the uncracked concrete due to elevated temperature; T_0 is the initial temperature; μ_c is the dynamic viscosity of the vapor-liquid mixture in cracks; δ_{NPj}^i denotes the facet normal crack openings on side T_i ($i = 1, 2$) in the FLE domain, $j = 1, 2, 3$; l_{NPj} is the crack length on the $\mathrm{P_1P_2P_3}$ surface (see in Fig. 2(c)).

D_4 is the thermal conductivity in Fourier's Law and $D_3 = 0$ is the coefficient for Dufour heat flux which is usually neglected due to its small contribution. As emphasized by Shen et al. [16], it is the cracks sub-orthogonal to thermal conduction, rather than the sub-parallel cracks, that have profound negative effect on concrete heat conduction performance. For this reason, the crack opening of 12 facets sub-orthogonal to FLE (Fig. 2(d)) are used to take into account the effect of fracture on the thermal conduction:

$$D_4 = \frac{\frac{l_{12}}{\lambda_w^0} + \frac{\bar{\delta}_{NO}^1}{\lambda_c} + \frac{\bar{\delta}_{NO}^2}{\lambda_c}}{l_{12} + \bar{\delta}_{NO}^1 + \bar{\delta}_{NO}^2} \tag{6}$$

in which, λ_w^0 is the initial thermal conductivity of uncracked material; $\bar{\delta}_{NO}^i = \sum_{j=1}^{6} \delta_{NOj}^i/6$ ($i = 1, 2$, $j = 1, 2, 3$) is the average normal cracking opening of the 6 facets sub-orthogonal to FLE on each side T_i; λ_c is the thermal conductivity of the vapor-liquid water mixture in the cracks.

$w_c(p, T)$ and $U_c(p, T)$ represent water mass and heat content per unit volume of cracked material and are calculated by the properties of the liquid-vapor water mixture in the cracks. These mixture properties are determined by the water state, because condensation and evaporation of free water might happen. If $h > 1.1$, water in the cracks is liquid. When $h < 1$, the water state is vapor. Otherwise, when $1 < h \leqslant 1.1$, water is a mixture and the phase change is modeled by the smoothstep function. $\chi_c = (\chi_l - \chi_v)\{-2[10(h-1)]^3 + 3[10(h-1)]^2\} + \chi_v$, in which χ_c, χ_v and χ_l are parameters for the vapor-liquid mixture, vapor and liquid water, respectively. The same function χ_c is used for ρ_c, C_c, λ_c, and μ_c in which ρ_l, ρ_v C_l, C_v, λ_l, λ_v, μ_l, μ_v can be found in [17].

3 Concrete thermal spalling mechanisms

This section analyzes the main mechanisms of concrete thermal spalling. The considered simulations setup (see in Fig. 3) is the one used in the experiments carried out by Lo Monte et al. [12]. In the numerical analyses a side length of 400 mm was used and, correspondingly, all other dimensions were scaled by 0.5. The heating load (Fig. 3) was applied on the central window (300×300 mm) and the displacements of the cold rim peripheral faces were set to zero. Since no information was available for the properties of the concrete used in the experiments, the parameters in Tab. 1 and Tab. 2 were used.

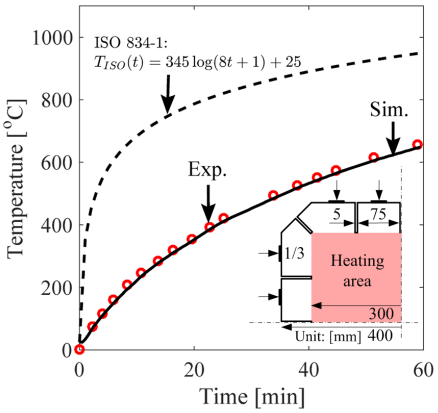

Figure 3: Spalling thermal loads and experiment setup.

Fig. 4 (a) and (b) show the crack opening distribution after 15 and 30 minutes of heating. After 15 minutes of heating, some initial spalling can be observed. As the temperature keeps increasing, the spalling area expands and many fragments are ejected from the surface. This phenomenon is similar to the high-speed cam-

era observations obtained by Zeiml et al. [4].

Table 2: Concrete mix-designs and model parameters used in the simulations

Para.	Unit	Concrete	Source
Mix-designs			
c	$[\mathrm{kg/m^3}]$	350	[11]
w_{mix}/c	[-]	0.5	[11]
a/c	[-]	5.23	[11]
d_a	[mm]	20	[11]
LDPM at room temperature			
E_0	[MPa]	43748	Identified
σ_t	[MPa]	4	Identified
l_t	[mm]	120	Identified
σ_s	[MPa]	10.8	Identified
σ_{c0}	[MPa]	150	Identified
μ_0	[-]	0.2	Identified
σ_{N0}	[MPa]	600	Identified
κ_{c0}	[-]	2	[9]
κ_{c1}	[-]	2	[9]
κ_{c2}	[-]	1	[9]
d_0	[mm]	4	Assumed
DTemPor3 model			
w_0	$[\mathrm{kg/m^3}]$	100	[2, 12]
D_w^0	$[\mathrm{m/s}]$	8×10^{-13}	Identified
λ_w^0	$[\mathrm{W/(^oC \cdot m)}]$	2	Identified
C_T	[-]	0.0045	Identified

The same numerical analyses were carried out again by excluding the effect of pressure ($b = 0$ in Eq. 3) or the effect of thermal expansion ($\alpha_T = 0$ in Eq. 1). Fig. 4 (c) shows the crack opening distribution after 30 minutes of heating if only thermal expansion is included. In this case the cracking distribution is similar to that of the complete simulation, but the spalling area is smaller and the generation of fragments is somewhat less pronounced. This indicates that thermal dilatation is a major contribution to generate damage inside the specimen and consequent spalling.

Fig. 4 (d) shows the crack opening distribution after 30 minutes of heating if only the effect of pressure is included. In this case, a totally different cracking pattern occurs. A clear macro-crack is formed near the heating surface which cannot be found in Fig. 4 (b) and much less micro-cracks are generated inside the specimen. The most important point is that no thermal spalling (fragment) is observed. In conclusion, it is clear that the effect of pressure is not enough to cause thermal spalling, but the formation of the macro-crack isolates a layer of concrete near the surface which is then more likely to buckle and to spall off if thermal stresses are present.

4 Conclusions

This study proposes a discrete 3D hygro-thermal model (DTemPor3) for concrete at high temperature coupled with the Lattice Discrete Particle Model (LDPM) for the simulation of thermal spalling. The two-way coupling simulations is equipped with the capability of taking into account the effect of cracks on heat transfer and mass transport as well as the cracking behavior caused by thermal expansion and pore pressure. This multi-physics framework is implemented into the MARS code [18].

By using the coupled the DTemPor3-LDPM framework, the numerical simulations reproduced successfully concrete thermal spalling. Thermal stresses play a dominant role in concrete thermal spalling. Thermal expansion supplies the major contribution to generate micro-cracks inside concrete. Pore pressure is not enough to form spalling, although pore pressure can form macro-cracks parallel to the heat surface which are then more likely to buckle and spall under the effect of thermal stresses.

REFERENCES

[1] Shorter G., and Harmathy T. 1965. Moisture clog spalling., *Proceedings of institution of civil engineers* **20** :75–90.

[2] Bažant, Z. P., and Kaplan, M. F. *Concrete at high temperatures: material properties and mathematical models,* Longman, 1996.

[3] Gawin, D., Pesavento, F., and Schrefler, B. 2006. Towards prediction of the thermal spalling risk through a multi-phase porous media model of concrete, *Computer meth-*

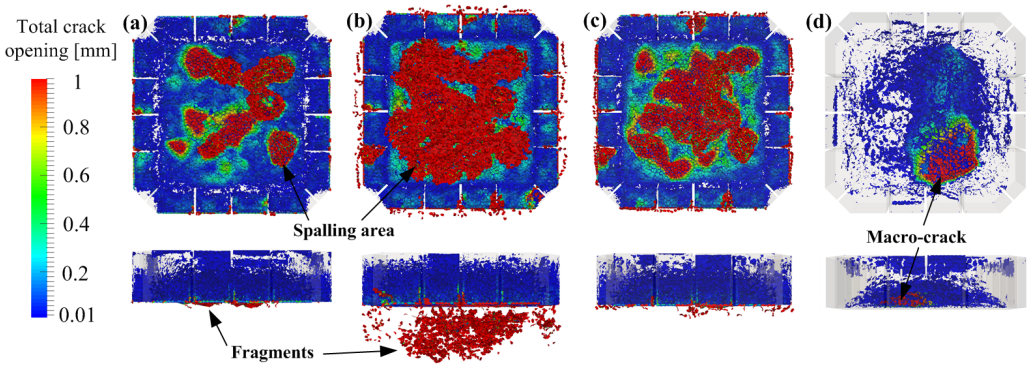

Figure 4: Crack opening contour during thermal spalling. (a) After 15 minutes of heating with all spalling factors included; (b) After 30 minutes of heating with all spalling factors included; (c) After 30 minutes of heating with only thermal stresses effect; (d) After 30 minutes of heating with only pressure effect.

ods in applied mechanics and engineering **195**: 5707–5729.

[4] Zeiml, M., Lackner, R., and Mang, H. A. 2008. Experimental insight into spalling behavior of concrete tunnel linings under fire loading, *Acta Geotechnica* **3**: 295–308.

[5] Tenchev, R., and Purnell, P. 2005., An application of a damage constitutive model to concrete at high temperature and prediction of spalling, *International Journal of Solids and Structures* **42**: 6550–6565.

[6] Davie, C. T., Pearce, C. J., and Bićanić, N. 2010. A fully generalised, coupled, multiphase, hygro-thermo-mechanical model for concrete, *Materials and structures* **43**: 13–33.

[7] Gawin, D., Pesavento, F., and Schrefler, B. A. 2011. What physical phenomena can be neglected when modelling concrete at high temperature? a comparative study. Part 1: Physical phenomena and mathematical model, *International journal of solids and structures* **48**: 1927–1944.

[9] Cusatis, G., Pelessone, D., and Mencarelli, A. 2011. Lattice discrete particle model (LDPM) for failure behavior of concrete. I: Theory, *Cement and Concrete Composites* **33**: 881–890.

[11] Kalifa, P., Menneteau, F. D., and Quenard, D. 2000. Spalling and pore pressure in hpc at high temperatures, *Cement and concrete research* **30**: 1915–1927.

[12] Monte, F. L., and Felicetti, R. 2017. Heated slabs under biaxial compressive loading: a test set-up for the assessment of concrete sensitivity to spalling, *Materials and Structures* **50**: 192.

[13] Biot, M. A. 1941. General theory of three-dimensional consolidation, *Journal of Applied Physics* **12**: 155–164.

[14] Grassl, P., and Bolander, J. E. 2016. Three-Dimensional Network Model for-Coupling of Fracture and Mass Transport in Quasi-Brittle Geomaterials, *Materials* **9**: 782–800.

[15] Di Luzio, G., and Cusatis, G. 2009. Hygro-thermo-chemical modeling of high performance concrete. I: Theory, *Cement and Concrete composites* **31**: 301–308.

[16] Shen, L., Ren, Q., Zhang, L., Han, Y., and Cusatis, G. 2017., Experimental and numerical study of effective thermal conductivity of cracked concrete, *Construction and Building Materials* **153**: 55–68.

[17] Yang, S.-M., and Tao, W.-Q. 2006. *Heat transfer theory*, High Education press.

[18] Pelessone, D. and Zhou, X. 2014. *MARS, Multiscale-multiphysics Analysis of the Response of Structures. Users manual*, ES3 Inc..